INSTITUTE OF PHYSICS PUBLISHING PHYSICS IN MEDICINE AND BIOLOGY

Phys. Med. Biol. **47** (2002) 1321–1332 PII: S0031-9155(02)25752-8

An analysis of MCNP cross-sections and tally methods for low-energy photon emitters

John J DeMarco, Robert E Wallace and Kirsten Boedeker

UCLA Department of Radiation Oncology, University of California, Los Angeles, 200 UCLA Medical Plaza, Suite B265, Los Angeles, CA 90095-6951, USA

E-mail: demarco@radonc.ucla.edu

Received 14 June 2001, in final form 21 February 2002
Published 5 April 2002
Online at stacks.iop.org/PMB/47/1321

Abstract

Monte Carlo calculations are frequently used to analyse a variety of radiological science applications using low-energy (10–1000 keV) photon sources. This study seeks to create a low-energy benchmark for the MCNP Monte Carlo code by simulating the absolute dose rate in water and the air-kerma rate for monoenergetic point sources with energies between 10 keV and 1 MeV. The analysis compares four cross-section datasets as well as the tally method for collision kerma versus absorbed dose. The total photon attenuation coefficient cross-section for low atomic number elements has changed significantly as cross-section data have changed between 1967 and 1989. Differences of up to 10% are observed in the photoelectric cross-section for water at 30 keV between the standard MCNP cross-section dataset (DLC-200) and the most recent XCOM/NIST tabulation. At 30 keV, the absolute dose rate in water at 1.0 cm from the source increases by 7.8% after replacing the DLC-200 photoelectric cross-sections for water with those from the XCOM/NIST tabulation. The differences in the absolute dose rate are analysed when calculated with either the MCNP absorbed dose tally or the collision kerma tally. Significant differences between the collision kerma tally and the absorbed dose tally can occur when using the DLC-200 attenuation coefficients in conjunction with a modern tabulation of mass energy-absorption coefficients.

1. Introduction

Monte Carlo methods have played an important role with respect to analysing the dosimetry parameters from low-energy photon emitters in the energy range of 1 to 1000 keV. This energy range is particularly relevant to the medical physics community because it covers a variety of dosimetry applications including low-energy brachytherapy (20–40 keV), diagnostic radiology (10–140 keV) and nuclear medicine (100–511 keV). The literature is replete with examples of various Monte Carlo codes used for low-energy photon calculations including the MCPT code of Williamson (1988), the EGS4 code and various

modifications of the original ETRAN code such as Cyltran, ITS and MCNP. The MCNP code developed and maintained at Los Alamos National Laboratory has become a useful simulation tool because of its ability to model coupled neutron–photon–electron transport using a generalized, three-dimensional simulation geometry. With respect to low-energy photon transport, MCNP has been used for a variety of radiological science applications including foetal dose assessment (Metzger and Van Riper 1999), SPECT simulations (Yanch and Dobrzeniecki 1993) and brachytherapy seed modelling (Wierzbicki *et al* 1998, DeMarco *et al* 1999, Rivard 2001). The purpose of this study is to evaluate the suitability of using MCNP4C for calculating the absorbed dose rate in water and the air-kerma strength as a function of monoenergetic photon source energy between 10 keV and 1 MeV. The calculations are performed using four different cross-section datasets and will also compare the absorbed dose tally versus a collision kerma tally.

2. The Monte Carlo code system

The MCNP4C Monte Carlo code is a general-purpose code capable of simulating coupled neutron–photon–electron problems using a three-dimensional heterogeneous geometry system (Briesmeister 1993). The conventional modelling package is based upon a combinatorial geometry system using planes, cylinders, cones and spheres to define the geometry. The detailed simulation of photon transport includes photoelectric absorption with the creation of K- and L-shell fluorescent photons or Auger electrons, coherent and incoherent scattering, and pair production. Electron binding effects associated with Compton and Rayleigh scatter are handled using the coherent and incoherent form factors of Hubbell (Hubbell *et al* 1975). The photoelectric cross-sections are based upon the tabulation of Storm and Israel (1967) and the scattering cross-sections taken from the ENDF tabulation (Hubbell *et al* 1975). Two different tally methods are available in MCNP for calculating the absorbed dose from low-energy photon emitters. The absorbed dose tally (*f8) scores the energy of each photon and electron upon entering and exiting the tally cell. This tally is a surface estimator and scores the net energy (MeV) deposited in a scoring region from the coupled photon–electron transport. The second method (*f4) scores the photon collision kerma by scoring the energy fluence and multiplying this value by an energy-dependent mass energy-absorption coefficient. The MCNP energy fluence tally (*f4) provides a track-length estimate of the energy fluence,

$$\Psi = \frac{EWT}{V}$$

where E is the photon energy (MeV), W the photon weight, T the track length through the tally cell and V the cell volume. This tally value is multiplied by a user-supplied table of mass energy-absorption coefficients to yield the absorbed dose assuming local energy deposition of secondary electrons.

3. Cross-section overview and study set-up

The study was designed for evaluating the ability of MCNP4C to calculate the absolute dose rate in water and the air-kerma rate from monoenergetic photon point sources. The monoenergetic point source calculations were compared with the published values of Luxton and Jozsef (1999). The authors used the EGS4 code to calculate the absolute dose rate, the air-kerma rate and the dose rate constant for monoenergetic point sources ranging from 10 keV to 2 MeV. For this study a maximum energy of 1 MeV was used in order to concentrate in the low-energy range of 20–40 keV. The latter energy range is relevant for ^{125}I and ^{103}Pd isotopes commonly used

for low-energy brachytherapy applications. The MCNP analysis was designed for evaluating the current MCNP4C photon cross-section tabulation for water versus three datasets: the 1970 compilation of Storm and Israel (DLC-015, Storm and Israel 1970), the 1989 HUGO VI tabulation (DLC-146, Trubey 1989) and the XCOM cross-section database maintained at the National Institute of Standards and Technology (Berger and Hubbell 1987, 1998/1999). The DLC datasets are distributed by the Radiation Safety Information Computational Center (RSICC) at Oak Ridge National Laboratory. The DLC-015 scattering cross-sections are based upon numerically integrating the Klein–Nishina and Thomson formulations weighted with the appropriate incoherent scattering functions (Cromer 1969) and atomic form factors for coherent scatter (Cromer 1968). The photoelectric cross-sections are tabulated based upon the work of Rakavy and Ron (1967) and Schmickley and Pratt (1967). The DLC-146 dataset is an update to the DLC-99/HUGO tabulation of Roussin *et al* (1983). The relativistic atomic form factors and corresponding photon coherent scattering cross-sections are taken from Hubbell and Øverbø (1979) and the incoherent scattering functions and incoherent cross-sections from Hubbell *et al* (1975). The major difference between DLC-146 and DLC-99 occurs with the photoelectric cross-sections. The DLC-99 photoelectric dataset is based upon the calculations of Scofield for all subshells, for all elements $Z = 1$ to 101, over the photon energy range 1 keV to 1.5 MeV with renormalization values for $Z = 2$ to 54 to convert to the relativistic Hartree–Fock model (Scofield 1973). After a comparison with the NIST measurement database, Saloman and Hubbell subsequently showed that the unrenormalized Scofield tabulation is a more appropriate photoelectric cross-section database and these values are used in the DLC-146 dataset (Saloman and Hubbell 1986). The XCOM program is an independent calculation algorithm which generates the incoherent and coherent scattering cross-sections using the method described above for the DLC-146 tabulation. For energies below 1.5 MeV the XCOM photoelectric cross-sections were obtained using the unrenormalized, phase-shift calculations of Scofield (1973).

The dose rate in water was calculated using MCNP4C for monoenergetic point sources ranging from 10 keV to 1 MeV. The *f8 energy deposition tally and the *f4 collision kerma tally were used to score the absorbed dose and collision kerma rate, respectively, in a spherical tally annulus of 0.1 mm radial thickness and 1.0 cm radial distance and a total phantom diameter of 40 cm. The detailed photon physics mode was used to transport primary photons and all secondary electrons and photons resulting from photoelectric, coherent and incoherent interactions based upon low-energy photon and electron cut-offs of 1 keV and 20 keV, respectively. The air-kerma strength as a function of monoenergetic source energy was calculated using the *f4 kerma tally. The calculation was performed in vacuum in a spherical tally annulus of 0.1 mm radial thickness and 1.0 cm radial distance. The mass energy-absorption coefficients for water and air as calculated by Seltzer and Hubbell (Seltzer 1993, Hubbell and Seltzer 1995) were used to modify the *f4 tally for the water-and air-kerma calculations, respectively. The photon and electron low-energy cut-offs were chosen to allow for direct comparison with the previously published EGS4 benchmark calculations of Luxton and Jozsef (1999). Hubbell provides an extensive overview of the mass attenuation coefficient and the current status of various compilations and comparisons (Hubbell 1999). The EPDL97 analysis from Cullen *et al* estimates an approximate uncertainty of 2% for the photoionization cross-section in the energy range of 5–100 keV (Cullen *et al* 1997).

4. Cross-section comparison

MCNP4C uses a master cross-section library file that contains the photoelectric, coherent scatter, incoherent scatter and pair-production cross-sections as well as scattering form factors

and fluorescence data. This library is designated as DLC-200 from RSICC at Oak Ridge National Laboratory. Three common tissue compounds (fat, water and cortical bone) were chosen for qualitative comparison between the RSICC and XCOM datasets. The elemental composition of the three compounds was taken from ICRU Report 44 (ICRU 1989). Figures 1(a)–(c) illustrate the total attenuation coefficient of the three tissue compounds as a function of cross-section dataset. The DLC-200 and DLC-015 cross-section tabulations for the four materials consistently underestimate the total mass attenuation coefficient relative to the XCOM dataset in the energy range of 10–60 keV. Figure 2 illustrates the comparison of the photoelectric interaction cross-section for water. The DLC-200 dataset tabulates a value that is smaller than XCOM by up to 10% at energies less than 100 keV. All cross-section comparisons are shown relative to the XCOM dataset because of its availability on the internet as shareware (http://physics.nist.gov/PhysRefData). The DLC datasets must be purchased separately from RSICC for a nominal fee. The MCNP4C/DLC-200 photon cross-section file was modified to accept the hydrogen and oxygen photoelectric cross-sections for each dataset (DLC-015, DLC-146 and XCOM). This allows a comparison of the absorbed dose rate and collision kerma rate to water as a function of cross-section tabulation.

5. Results

5.1. Absorbed dose rate calculations for monoenergetic photon point sources in water

Figure 3 illustrates the relative comparison of the MCNP4C calculations using the DLC-200, DLC-015 and DLC146 cross-section datasets versus the XCOM dataset. The EGS4 calculations of Luxton and Jozsef (1999) are also shown relative to the MCNP4C/XCOM calculation. The MCNP4C calculations are performed until a standard error of less than 1% is achieved using the energy deposition tally (*f8). For the energy range between 20 and 40 keV the absorbed dose rate calculation performed using the DLC-200 cross-sections underestimates the dose rate at 1.0 cm by an average of 6.3% and a maximum value of 7.8% (40 keV) relative to the XCOM dataset. At 10 keV the DLC-200 and DLC-015 datasets overestimate the absorbed dose rate by 25% and 17%, respectively. The agreement between MCNP4C/DLC-015 and the EGS4/DLC-015 calculations of Luxton and Jozsef (1999) is very good with small differences probably due to differences in the underlying electron and photon transport algorithms.

5.2. Collision kerma rate calculations for monoenergetic photon point sources in water

Figure 4 illustrates the relative comparison of the water collision kerma rate (*f4 tally) using the DLC dataset versus the XCOM cross-sections. The *f4 calculations were performed until a standard error of less than 1% was achieved. The DLC-200 dataset overestimates the water kerma rate by 33% at 10 keV and 2.3% at 30 keV. Figure 5 compares the MCNP4C calculations for the energy deposition tally (*f8) versus the water collision kerma tally (*f4) as a function of cross-section tabulation. Using the DLC-200 and DLC-015 cross-section data the collision kerma rate is consistently greater than the absorbed dose rate between 10 and 100 keV. This is because the *f4 tally calculates the photon energy fluence using the DLC-200 and DLC-015 attenuation coefficients and converts to collision kerma using the mass energy-absorption coefficients of Seltzer and Hubbell (Seltzer 1993, Hubbell and Seltzer 1995). This μ_{en}/ρ tabulation is based upon the DLC-146 or XCOM cross-sections, thus producing an inconsistent kerma calculation.

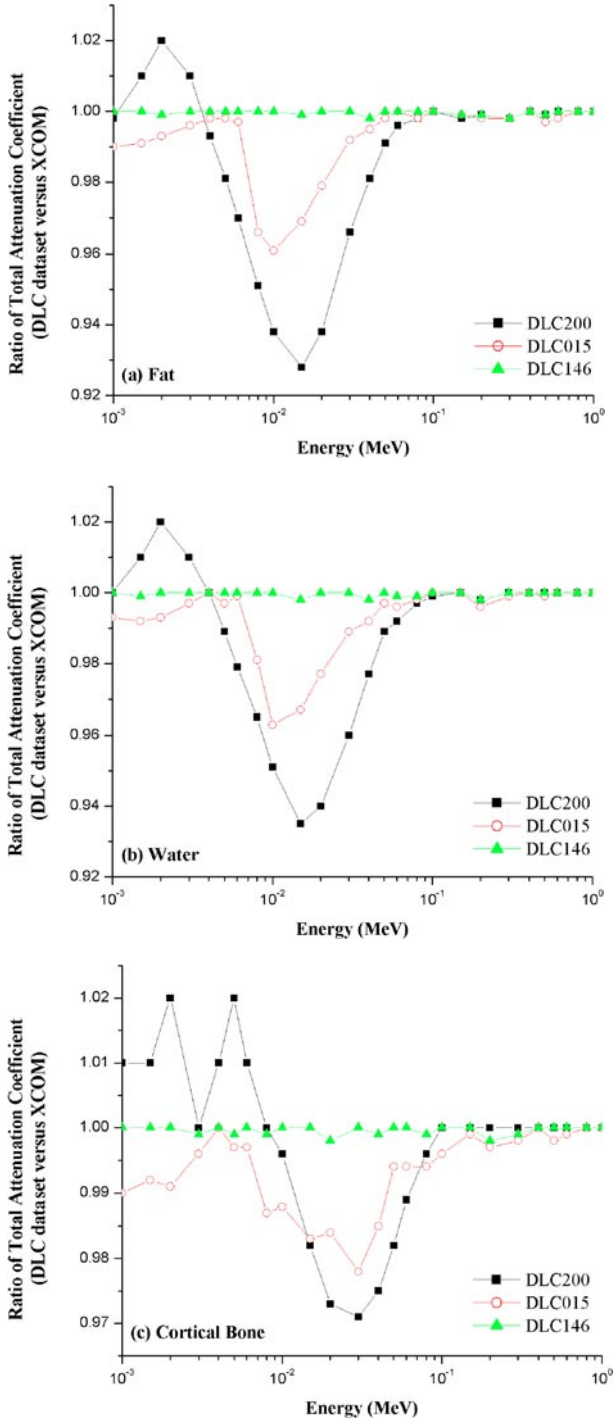

Figure 1. Comparison of the DLC-200, DLC-015 and DLC-146 tabulation for the total mass-attenuation coefficient of fat (a), water (b) and coritical bone (c) versus the XCOM tabulation.

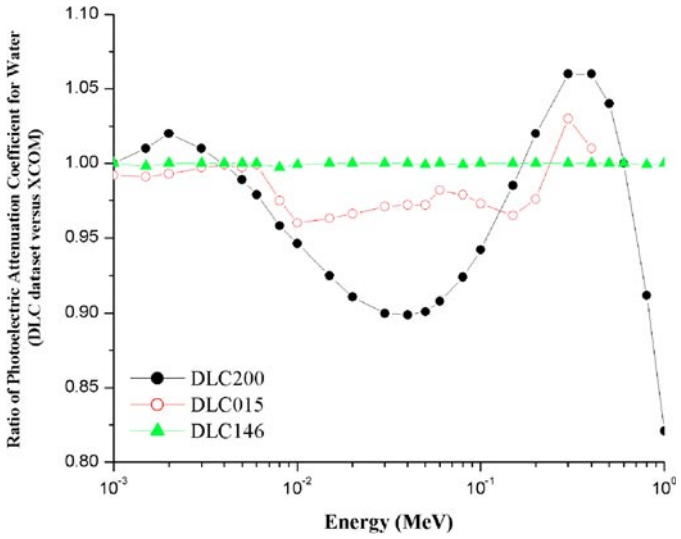

Figure 2. Comparison of the DLC-200, DLC-015 and DLC-146 photoelectric interaction cross-sections versus the XCOM tabulation for water.

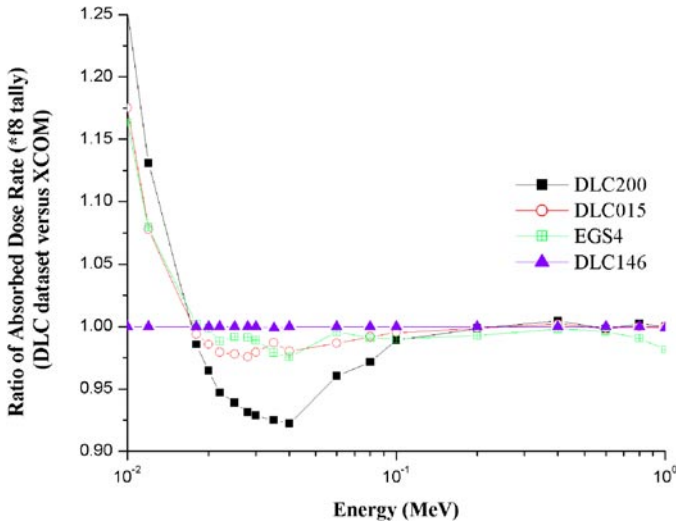

Figure 3. Relative comparison of MCNP4C calculations as a function of DLC cross-section dataset versus XCOM tabulation for the absolute dose rate at 1.0 cm from monoenergetic photon point sources in water. The MCNP calculations are performed using the*f8 absorbed dose tally. The EGS4 calculations of Luxton and Jozsef are also shown for comparison.

5.3. Air-kerma rate calculations for monoenergetic photon point sources

The air-kerma strength calculation was calculated using the *f4 energy fluence tally and the mass energy-absorption coefficients for air from Seltzer and Hubbell (Seltzer 1993, Hubbell and Seltzer 1995). Figure 6 illustrates the comparison between the MCNP4C simulations and the hand calculations of Luxton and Jozsef (1999). The MCNP4C simulation systematically overestimates the air-kerma relative to the Luxton calculation by an average of 1.024 ± 0.11% for the energy range of 20–40 keV. This is due to the different mass

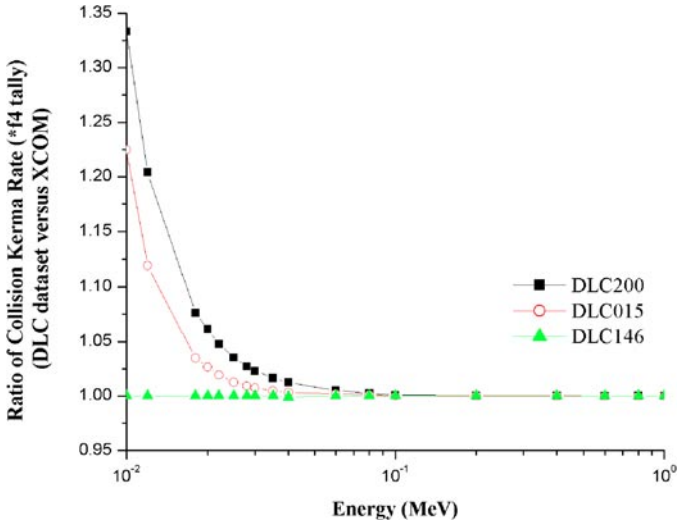

Figure 4. Relative comparison of MCNP4C calculations as a function of DLC cross-section dataset versus the XCOM tabulation for the water collision kerma rate at 1.0 cm from monoenergetic photon point sources in water. The MCNP4C calculations are performed using the *f4 energy fluence tally and the tabulation of mass energy-absorption coefficients for water from Hubbell and Seltzer (1995).

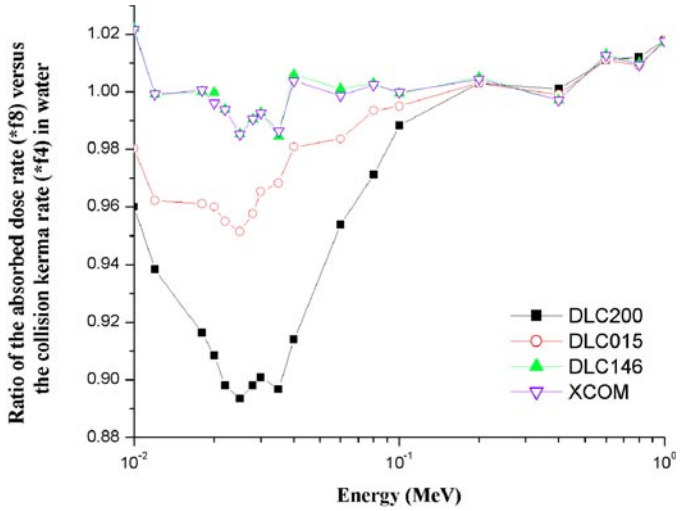

Figure 5. Relative comparison of the MCNP4C absorbed dose tally (*f8) versus the *f4 collision kerma tally as a function of cross-section dataset at a radial distance of 1.0 cm from monoenergetic photon point sources in water.

energy-absorption cross-sections for air. Luxton and Jozsef use the 1982 μ_{en}/ρ tabulation of Hubbell (1982). The MCNP4C air-kerma calculations were performed using the 1995 μ_{en}/ρ tabulation of Seltzer and Hubbell (Seltzer 1993, Hubbell and Seltzer 1995). The air-kerma ratio mirrors the ratio of the corresponding mass energy-absorption coefficients for air.

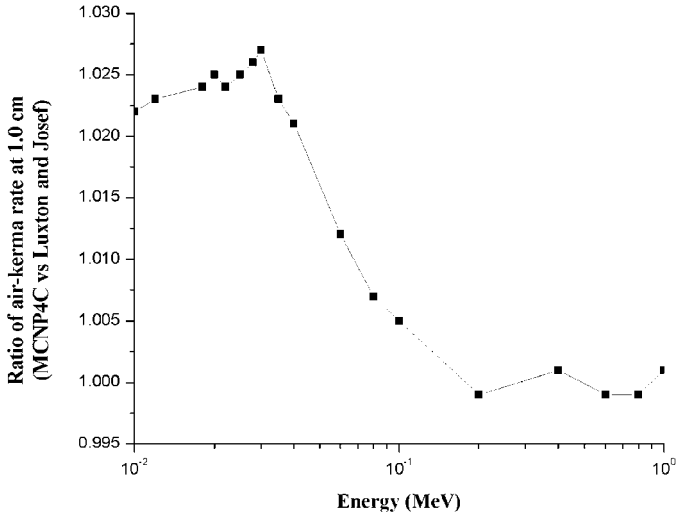

Figure 6. Relative comparison of MCNP4C air-kerma rate calculations versus the analytical calculations of Luxton and Jozsef (1999) for the air-kerma strength of monoenergetic photon point sources in vacuum. The calculation is performed at a radial distance of 1.0 cm.

6. Discussion

The cross-section tabulation affects the transport of photons through the medium and therefore the relative number of photons and secondary electrons (if applicable) crossing a scoring region. An overview of the underlying tally method is necessary for understanding the above differences. The MCNP absorbed dose tally (*f8) is considered a surface estimator and will score the energy deposited only if there is a photon interaction within the annulus or when an electron crosses into the tally cell. With respect to photons, the scoring routine is called initially when the photon crosses the inner radial surface and the photon energy is added to the cell tally. The routine is called a second time when (if) the photon crosses the outer radial surface. If the photon does not have an interaction the net energy absorbed is zero. The behaviour of the absorbed dose tally (*f8) as a function of cross-section dataset can be evaluated by analysing the transport of primary photons only. We modified the code to compare the total number of photon interaction events per history via a user-defined flag that is set within the MCNP input file. When the event flag is set to zero the code completes the transport of any secondary electrons associated with the first interaction event and terminates the primary photon history. When the flag is set to a non-zero integer, n, the transport terminates with the history of the nth order of scatter. The probability of a primary photon collision in the tally annulus is equal to $(e^{-\mu x_1}) \cdot (1 - e^{-\mu x_2})$. The first term represents the probability that a primary photon reaches the inner surface of the tally annulus without interacting ($x_1 =$ 1.0 cm) and the second term represents the probability that the photon has an interaction in the tally annulus ($x_2 = 0.01$ cm). The MCNP4C simulation for absorbed dose in the annulus from primary interactions only versus the analytical relationship discussed above is listed in table 1 . The DLC200 and XCOM datasets were used for the comparison. The analytical relationship and primary-only Monte Carlo simulation agree quite well over the energy range of 10–100 keV. The total absorbed dose in the tally annulus from primary and scatter photons predicts a larger difference between the DLC200 and the XCOM datasets. For a 30 keV photon the difference in the cross-section data produces a 2.4% and 7.1% absorbed

Table 1. Comparison of MCNP calculations for primary and primary+scatter versus the analytical behaviour of the absorbed dose and collision kerma tally for primary photons in water ($x_1 = 1.0$ cm; $x_2 = 0.01$ cm).

	Absorbed dose tally ratio (DLC200/XCOM)			Collision kerma tally ratio (DLC200/XCOM)		
Energy (keV)	MCNP (primary)	MCNP (primary+scatter)	Analytic $(e^{-\mu x_1}) \cdot (1 - e^{-\mu x_2})$	MCNP (primary)	MCNP (primary+scatter)	Analytic $(e^{-\mu x_1})$
10	1.258	1.253	1.236	1.326	1.333	1.298
20	0.987	0.965	0.987	1.050	1.061	1.050
30	0.976	0.929	0.974	1.014	1.023	1.015
40	0.984	0.922	0.985	1.006	1.013	1.006
60	0.995	0.960	0.994	1.001	1.005	1.002
80	0.998	0.972	0.996	1.000	1.003	1.001
100	0.999	0.989	0.997	1.000	1.001	1.001

dose difference assuming primary and primary+scatter, respectively. Equation (1) extends the primary-only, analytical approximation by evaluating the absorbed dose in the scoring annulus as the number of photons interacting in the annulus times the average energy transferred to secondary electrons per photon interaction.

$$D \propto e^{-\mu x_1}(1 - e^{-\mu x_2})\overline{h\nu}\left(f_{PE}\frac{\mu_{PE}}{\mu} + f_{INCOH}\frac{\mu_{INCOH}}{\mu}\right). \tag{1}$$

Equation (1) can be simplified by noting that $1 - e^{-\mu x_2} \approx \mu x_2$ since $x_2 \ll 1/\mu$. Because our attenuation medium is water we can also assume that the production of fluorescent photons is negligible following a photoelectric event ($f_{PE} = 1$). We can approximate $f_{INCOH} = \sigma_{tr}/\sigma$ assuming the standard Klein–Nishina theory for photon scatter from an unbound electron where σ_{tr} represents the Klein–Nishina energy-transfer cross-section and σ the total Klein–Nishina cross-section per electron.

$$D \propto e^{-\mu x_1} x_2 \overline{h\nu}\left(\mu_{PE} + \frac{\sigma_{tr}}{\sigma}\mu_{INCOH}\right). \tag{2}$$

Based upon equation (2), the ratio of the absorbed dose in the scoring annulus as a function of the DLC-200 versus XCOM cross-section dataset is therefore

$$\frac{D_{DLC200}}{D_{XCOM}} \approx e^{-x_1(\mu_{DLC200} - \mu_{XCOM})} \frac{\left(\mu_{PE}^{DLC200} + \frac{\sigma_{tr}}{\sigma}\mu_{INCOH}^{DLC200}\right)}{\left(\mu_{PE}^{XCOM} + \frac{\sigma_{tr}}{\sigma}\mu_{INCOH}^{XCOM}\right)}. \tag{3}$$

We evaluated the photon fluence spectrum using MCNP and found that the average photon energy within the annulus changed by less than 0.2% for the DLC-200 versus XCOM datasets, allowing the cancellation of the average initial photon energy term. Table 2 compares the behaviour of equation (3) versus the MCNP primary+scatter calculation and shows good agreement between the two methods. This indicates that the relative interaction probability of the photoelectric effect versus the total attenuation coefficient accounts for the differences observed between the primary and primary+scatter absorbed dose simulations in table 1.

In contrast to the absorbed dose tally, the *f4 tally overestimates the kerma as the cross-sections are changed from DLC-200 to DLC-146. The behaviour of the collision kerma tally is basically a function of the photon fluence within the annulus where the probability of a primary photon reaching the tally annulus without interacting is equal to $e^{-\mu x}$ ($x = 1.0$ cm). As described previously the mean photon energy within the scoring annulus is approximately independent of the cross-section dataset and therefore the photon energy and mass energy-absorption coefficients cancel when taking the ratio of collision kerma as a function of dataset.

Table 2. Comparison of MCNP calculations for primary+scatter versus the analytical approximation (equation (3)) accounting for energy transferred to charged particles from a photoelectric or incoherent scatter interaction in the tally cell. The ratio σ_{tr}/σ represents the average fraction of the incident photon's energy transferred to a Compton recoil electron.

Monoenergetic source energy (keV)	Mean photon energy at 1.0 cm (keV)	σ_{tr}/σ	Total attenuation coefficient ($cm^2\ g^{-1}$)		Photoelectric attenuation coefficient ($cm^2\ g^{-1}$)		Absorbed dose tally ratio (DLC200/XCOM)	
			DLC200	XCOM	DLC200	XCOM	Analytic	MCNP
10	10.0	0.019	5.070	5.330	4.70×10^{0}	4.97×10^{0}	1.228	1.253
20	19.8	0.036	0.761	0.810	5.12×10^{-1}	5.63×10^{-1}	0.958	0.965
30	29.3	0.051	0.361	0.376	1.42×10^{-1}	1.58×10^{-1}	0.919	0.929
40	38.5	0.065	0.262	0.268	5.75×10^{-2}	6.41×10^{-2}	0.919	0.922
60	56.7	0.089	0.204	0.206	1.63×10^{-2}	1.80×10^{-2}	0.952	0.960
80	74.7	0.111	0.183	0.184	6.67×10^{-3}	7.26×10^{-3}	0.978	0.972
100	92.5	0.130	0.170	0.171	3.34×10^{-3}	3.58×10^{-3}	0.991	0.989

This is consistent with the collision kerma ratio presented in table 1, where the analytical relationship and the Monte Carlo simulations agree quite well for the case of primary and primary+scatter as a function of the DLC-200 and XCOM cross-sections.

As previously discussed in section 5.2, the relative difference between the absorbed dose and collision kerma tallies becomes worse for older cross-section datasets due to inconsistent transport cross-sections and mass energy-absorption coefficients. The absorbed dose tally is smaller by an average value of 10% relative to the collision kerma tally over the energy range of 20–40 keV when using the DLC-200 cross-section data. When the transport cross-sections are updated to the DLC-146 or XCOM tabulations the ratio of absorbed dose to kerma is approximately equal to 1 within the statistical uncertainty (≈1–2%) of the calculations. This is to be expected since the transport cross-sections are equivalent to the cross-sections used in the μ_{en}/ρ tabulation of Hubbell and Seltzer (1995). This is of particular importance to any future work evaluating the equivalence of absorbed dose and collision kerma and emphasizes the need for consistent and modern attenuation and energy-absorption coefficients.

7. Conclusion

While MCNP is widely used for a variety of medical physics applications, the potential user must be aware of limitations for simulating in the low-energy regime of 10–100 keV. Using the standard DLC-200 cross-section distribution MCNP4C will underestimate the absolute dose rate of monoenergetic photon point sources in water relative to modern cross-section tabulations (DLC-146 or XCOM) for the energy range of 20–100 keV while the opposite is true for the energy range of 10–20 keV. The major differences in the cross-section datasets for the low-Z materials evaluated in this study occur with the photoelectric cross-sections. Differences are also observed when scoring the water collision kerma rate as a function of the cross-section dataset and comparing these values with the absorbed dose tally. The most significant discrepancy occurs when scoring the energy fluence rate in water with the DLC-200 attenuation cross-sections and multiplying this value with a modern tabulation of water mass energy-absorption coefficients. It is clear from this analysis that the choice of cross-section dataset can significantly influence the absolute dose rate in water for monoenergetic photon point source emitters. For low-energy brachytherapy calculations in the energy range of

10–100 keV the photoelectric coefficients in the MCNP4C/DLC-200 cross-section distribution should be updated to a modern tabulation such as DLC-146 or XCOM.

Acknowledgments

The authors gratefully acknowledge the time and effort expended in the review process from an anonymous referee. His/her detailed comments and suggestions have significantly improved the final version of this paper.

References

Berger M J and Hubbell J H 1987 XCOM: photon cross-sections on a personal computer *NBSIR 87-3597* (Washington, DC: NBS)

Berger M J and Hubbell J H 1998/1999 Photon attenuation coefficients *CRC Handbook of Chemistry and Physics* 79th edn, ed D R Lide (Boca Raton, FL: CRC Press) pp 10-207

Briesmeister J F 1993 MCNP—a general Monte Carlo N-particle transport code, version 4B *Los Alamos National Laboratory Report* LA-12625

Cromer D T 1968 X-ray scattering factors computed from numerical Hartree–Fock wave functions *Acta Crystallogr.* A **24** 321–4

Cromer D T 1969 Compton scattering factors for aspherical free atoms *J. Chem. Phys.* **50** 4857–9

Cullen D E, Hubbell J H and Kissel L 1997 EPDL97: the evaluated photon data library *Lawrence Livermore National Laboratory Report* UCRL-50400, vol 6, rev 5

DeMarco J J, Smathers J B, Burnison C M, Ncube Q K and Solberg T D 1999 CT-based dosimetry calculations for ^{125}I prostate implants *Int. J. Radiat. Oncol. Biol. Phys.* **45** 1347–53

Hubbell J H 1982 Photon mass attenuation and energy-absorption coefficients from 1 keV to 20 MeV *Int. J. Appl. Radiat. Isot.* **33** 1269–90

Hubbell J H 1999 Review of photon interaction cross section data in the medical and biological context *Phys. Med. Biol.* **44** R1–R22

Hubbell J H and Øverbø I 1979 Relativistic atomic form factors and photon coherent scattering cross-sections *J. Phys. Chem. Ref. Data* **8** 69–105

Hubbell J H and Seltzer S M 1995 Tables of x-ray mass attenuation coefficients and mass energy-absorption coefficients 1 keV to 20 MeV for elements $Z = 1$ to 92 and 48 additional substances of dosimetric interest *NISTIR 5632*

Hubbell J H, Veigele W J, Briggs E A, Brown R T, Cromer D T and Howerton R J 1975 Atomic form factors, incoherent scattering functions, and photon scattering cross-sections *J. Phys. Chem. Ref. Data* **4** 471–538 (erratum in **6** 615–6 (1977))

ICRU 1989 Tissue substitutes in radiation dosimetry and measurement *ICRU Report* 44 (Bethesda, MD: ICRU)

Luxton G and Jozsef G 1999 Radial dose distribution, dose to water and dose rate constant for monoenergetic photon point sources from 10 keV to 2 MeV: EGS4 Monte Carlo model calculation *Med. Phys.* **26** 2531–8

Metzger R L and Van Riper K A 1999 Fetal dose assessment from invasive special procedures by Monte Carlo methods *Med. Phys.* **26** 1714–20

Nath R, Anderson L L, Luxton G, Weaver K A, Williamson J F and Meigooni A S 1995 Dosimetry of interstitial brachytherapy sources: recommendations of the AAPM Radiation Therapy Committee Task Group No 43 *Med. Phys.* **22** 209–34

Rakavy G and Ron A 1967 Atomic photoeffect in the range $E\gamma = 1$–2000 keV *Phys. Rev.* **159** 50–6

Rivard M J 2001 Monte Carlo calculations of AAPM Task Group Report No 43 dosimetry parameters for the MED3631-A/M ^{125}I source *Med. Phys.* **28** 629–37

Roussin R W, Knight J R, Hubbell J H and Howerton R J 1983 Description of the DLC-99/HUGO package of photon interaction data in ENDF/B-V format *ORNL/RSIC-46/END-335*

Saloman EB and Hubbell J H 1986 X-ray attenuation coefficients (total cross sections): comparison of the experimental data base with the recommended values of Henke and the theoretical values of Scofield for energies between 0.1–100 keV *NBSIR 86-3431* (Washington, DC: NBS)

Schmickley R D and Pratt R H 1967 K-, L-, and M-shell atomic photoeffect for screened-potential models *Phys. Rev.* **164** 104–16

Scofield J H 1973 Theoretical photoionization cross sections from 1 to 1500 keV *Lawrence Livermore National Laboratory Rep* UCRL-51326

Seltzer S M 1993 Calculation of photon mass energy-transfer and mass energy-absorption coefficients *Radiat. Res.* **136** 147–70

Storm E and Israel H I 1967 Photon cross-sections from 0.001 to 100 MeV for elements 1 through 100 *Los Alamos Scientific Laboratory Report* LA-3753

Storm E and Israel H 1970 Photon cross-sections from 1 keV to 100 MeV for elements $Z = 1$ to $Z = 100$ *Nucl. Data Tables* A **7** 566–75

Trubey D K 1989 HUGI VI notes documentation for the DLC-146 code package Radiation Safety Information Computational Center

Wierzbicki J G, Rivard M J, Waid D S and Arterbery V E 1998 Calculated dosimetric parameters of the IoGold ^{125}I source model 3631-A *Med. Phys.* **25** 2197–9

Williamson J F 1988 Monte Carlo evaluation of specific dose constant in water for ^{125}I seeds *Med. Phys.* **15** 686–94

Yanch J C and Dobrzeniecki A B 1993 Monte Carlo simulation in SPECT: complete 3D modeling of source, collimator, and tomographic data acquisition *IEEE Trans. Nucl. Sci.* **40** 198–203